

Haukur Ingason

Modelling of Two Dimensional Rack Storage Fires

BRANDFORSK project 701-917

Haukur Ingason

Modelling of Two Dimensional Rack Storage Fires

BRANDFORSK project 701-917

Abstract

A theoretical model to predict mass flow rate, temperature, velocity and flame height in a two dimensional rack storage has been developed. Experiments have been carried out using inert boxes and a diffusion propane line burner located at the bottom of the rack. A reasonably good correlation is found between the model and the experiments.

The theoretical model developed calculates the flow within the rack with the aid of the equations of continuity, momentum and energy. The model distributes fractions of the total convective heat from the burner along a calculated flame height in accordance with an empirical relationship obtained from measured convective heat at each tier. The flame height is calculated by comparing the amount of available air flow rate and fuel rate at each tier for different heat release rates and widths of the flues.

The results were compared to experiments with an approximately two dimensional, 4 tier rack storage with height ranging from 1.14 m to 1.34 m and with a 0.59 m long diffusion line burner placed at the bottom of the vertical flue. The size of the rack is about 1/3 of what can be expected in a real rack storage.

Key words: rack storage, modelling, flame height, line burner, propane

SP

SP Rapport 1993:57
ISBN 91-7848-443-X
ISSN 0284-5172
Borås 1993

**Swedish National Testing and
Research Institute**
SP REPORT 199X:XX

Postal address:
Box 857, S-501 15 BORÅS,
Sweden
Telephone + 46 33 16 50 00
Telex 36252 Testing S
Telefax + 46 33 13 55 02

Table of Content		page
	Abstract	2
	Table of Content	3
1	Introduction	4
2	Background	4
3	The theoretical model	6
3.1	The continuity equation	10
3.2	The energy equation	10
3.3	Calculation of pressure drop	12
3.3.1	Pressure drop at the first tier	13
3.3.2	Pressure drop at intermediate tiers	17
3.3.3	Pressure drop at the highest tier	20
3.3.4	Pressure calculations after the first round	20
3.4	The flame height	21
3.5	Distribution of the convective heat energy	23
4	Experimental set-up	25
5	Results	26
6	Conclusions	33
7	Acknowledgement	33
8	Nomenclature	34
9	References	36

1 Introduction

Fire growth rate and flame propagation are dependent on how the burning material is stored. In rack storage fires this becomes extremely important as the upward flame propagation is usually very rapid. The flues created between adjacent pallets of stored goods tend to work as chimneys and subsequently they enhance acceleration of flames up to the ceiling. Rack storage fire protection usually consists of in-rack sprinklers which are placed at different elevations in the vertical flues or on the faces of the rack storage. The efficiency of such protection measures depends on the geometry of the stored goods, their height, the flue spacing and the flammability of the stored goods. The time over which the in-rack sprinkler operates is extremely important as it may be critical for control of the fire. To calculate the response-time a knowledge of the flow conditions close to the sprinkler is necessary. A theoretical model which can predict the flow conditions is thus of interest. Such a model could benefit to the optimisation of geometrical parameters in large rack storage in regard to sprinkler location. However, no simple theoretical models have been available to predict the flow conditions. In the present study the first step is taken to create a model which can be used to calculate the flow conditions in a two dimensional rack storage.

The phenomena governing the flame spread in rack storage fires are not well known. To the best of the author's knowledge no attempts to model flame spread in rack storage fires have been undertaken. Such modelling work could enhance the understanding of the fire propagation and the air entrainment mechanism in rack storage fires. One key aspect here is to obtain a knowledge about the effects of different flue sizes on both flow conditions and flame spread. A fully developed rack storage model could be used to predict fire growth rates and response times of in-rack sprinklers for different rack storage configurations. To establish a model like that, several steps must be undertaken, starting with simple geometries and simple combustion processes.

It was decided to concentrate the modelling work on the fluid dynamic part of rack storage fires, as the flame spread problem in rack storage fires is very complicated, and still not completely solved for even simpler cases. To accomplish that experiments with inert boxes in a scale one to three of a real rack storage in two dimensional configuration were carried out [1]. The work presented here is included in a project sponsored by the Swedish Fire Research Board (BRANDFORSK) aimed to obtain a better knowledge about rack storage fires and to establish a model which can predict the response of in-rack sprinklers in different rack storage configurations.

2 Background

Models for buoyancy driven flows (created by a fire) in vertical stacks or shafts can be found in various studies [2,3,4]. The present work differs from these studies in that a rack storage usually consists of a multi-stack system (vertically) and not of a single stack. The flow within each stack (flue) is governed by corresponding equations as for a single stack. However, the boundary conditions at the ends of each flue, i.e. at the intersections between the tiers, are quite different.

Heskestad and Yu [2] determined the convective flow in a combustible circular stack with a simple model. The model is assumed to be valid until the material on the wall ignites. The model assumes that the inflowing cold air at the base of the stack is heated up by a fire (which is located just below the base) over a shallow height just inside the stack, raising the gas temperature from ambient to a bulk

temperature. The temperature inside the stack is assumed to be uniform over its height. The air velocity at the inlet of the stack, created by the draft in the stack, is determined from a relationship developed by Delichatsios [3]. The velocity is derived from the momentum equation, assuming turbulent conditions in the stack. The static pressure at the top of the stack is assumed to be equal to the atmospheric pressure at the same elevation.

Block [4] worked with a theoretical model for burning rate of wood cribs. A wood crib consist of cross piled wood sticks which create vertical rectangular shafts with side holes along the height of the shafts. Although a wood crib is by its construction comparable to a rack storage, Block made an assumption in his model which has not been applied in the present study, namely, that all the air entering the vertical shafts enters at the bottom of the wood crib. However, a simple model presented in Ref. [1] shows that this assumption is justified for two dimensional rack storage when the mass flow rate at the top of the rack is the parameter of interest. But in the case of wood cribs, the air is drawn naturally through the side holes into the vertical shaft but according to Block [3] the majority of the air enters near the bottom. Consequently, he was able to assume a constant mass flow and density throughout the interior of the shaft. He also showed that the resistance on the vertical flow in the shaft created by the air entering the side holes can be neglected for wood cribs.

Ingason [1,5] reported on 1/3 scale tests both in three dimensional and two dimensional configurations with inert boxes. The most interesting conclusions drawn from [1] are: the width of the vertical flue is the predominant geometrical parameter controlling the flue flow; the mass flow rate increases nearly linearly with the width, the effects of the horizontal flue heights are small; for a certain flue width, the mass flow rate in the vertical flue is nearly constant, independent of the heat output. In Ref. [5] it was concluded that the flame heights tend to be lower in the three dimensional case than in the two dimensional case. A possible explanation is that the air is more easily entrained in the three dimensional case.

Karlsson et. al.[6] made similar experiments on reduced scale (1/3) to examine the geometrical effects on the flame height. Correlations presented by Karlsson et. al.[6] for flame heights clearly show that the effects of the horizontal flue heights are small. There is a certain difference in the flame height data between Ref. [5] and [6]. The difference is probably due to variations in the experimental set-up. In [6] the rack was four boxes wide and five boxes high with one side open while in [5] the rack was only two boxes wide and four boxes high, configured in two and three dimensions, respectively.

The study presented here is the second phase in the development of a model to predict the flue flow within a two dimensional rack storage. The first phase contained analysis of the data and description of the experimental set-up [1].

3 The theoretical model

The theoretical model is based on simple relationships from fluid dynamics. It can be used for inert environment in two dimensional (2-D) rack storage configurations as shown in Figure 1. The rack storage is shown in three views.

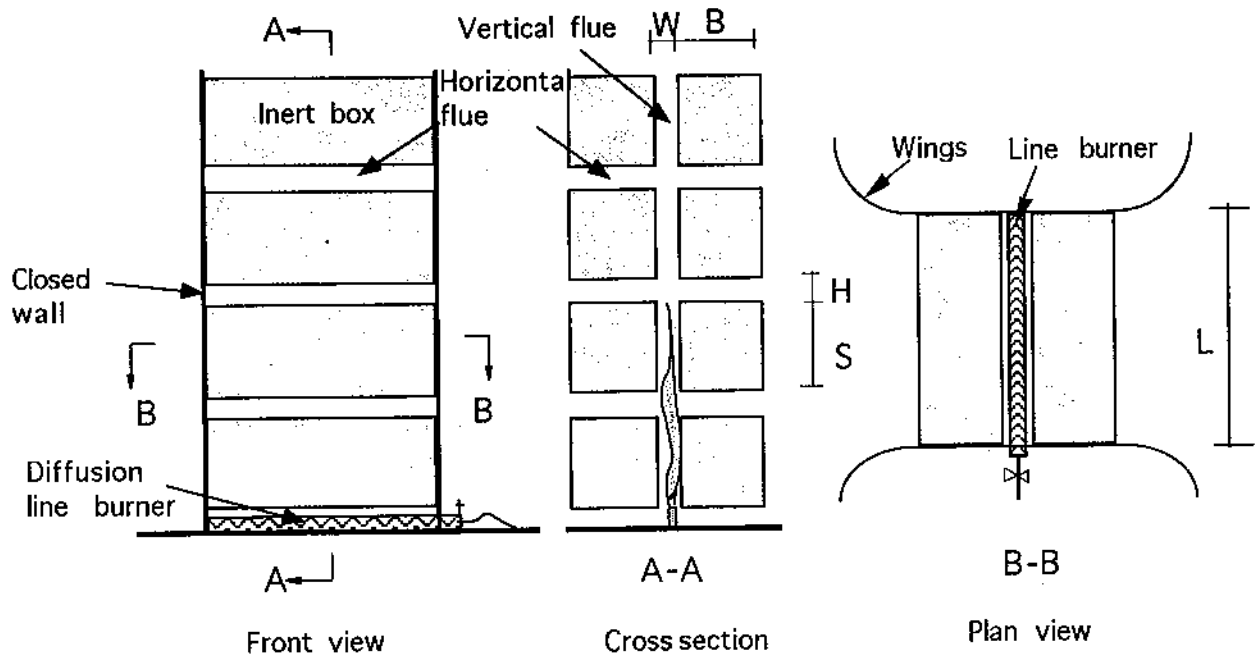


Figure 1 A simple theoretical model is developed to predict the velocity, temperature, mass flow rate and flame height in the flues in a 2-D rack storage as shown in the figure. Three different views of the rack are shown. The wings shown in the plan view were used to obtain a uniform air inflow into the horizontal flues.

The model predicts mass flow rate, temperature, velocity and flame height in the flues. The conditions within the flues are assumed to be steady-state and the flow is turbulent. Temperature, velocity and mass flow rate are represented by a mean value across the cross section of the flue. The input parameters used in the model are:

- the longitudinal length of the rack (L)
- the height and the width of the boxes, (S) and (B), respectively
- the width of the vertical flue (W)
- the height of the horizontal flues (H)
- the convective heat energy released from the propane line burner at the floor (Q_c).

In the work on combustible stacks, Heskestad and Yu [2] basically assumed a point source just inside the inlet of the stack. This approach has been modified here as the flames usually extend over several boxes in height. It is known from measurements carried out by Tamanini [7] on buoyancy-controlled open flames that the cumulative fraction of the total heat energy release within the flame increases as a function of height. These measurements show that above about half of the flame height (for a propane fire) most of the chemical heat energy has been released. Based on this knowledge it was justified to establish a method to describe the energy release along the flame height, i.e. to establish a relationship where the distribution of convective heat energy release is given as a function of height from the floor.

Figure 2 outlines how the total convective heat release is determined along the flame height. The derivation of the relationship $Q_c(z)$ is given in detail in Chapter 3.5.

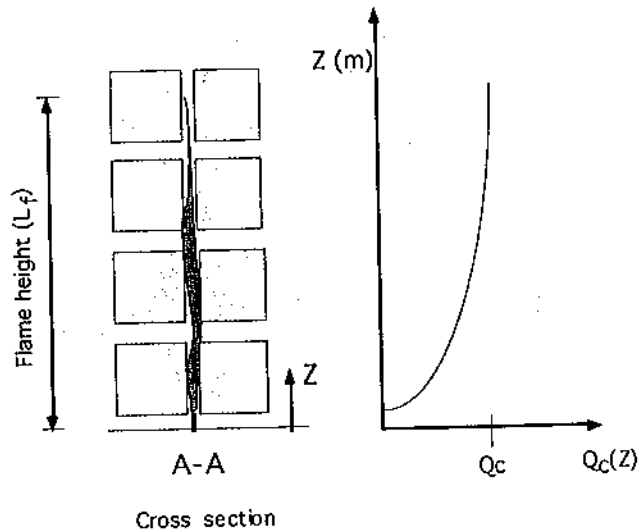
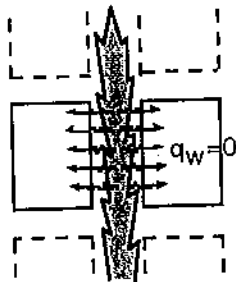


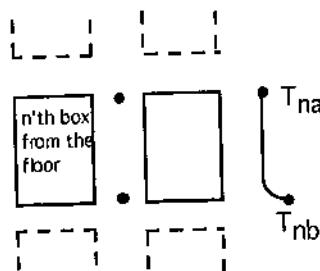
Figure 2 The total convective heat energy (Q_c) from the burner is released as a function of height in the model. This is schematically shown by the diagram.

In the theoretical model the following assumptions have been made:

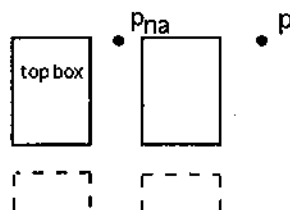
- 1) No convective heat losses are assumed in the vertical flue. This means that the heat transferred to the walls (q_w) by convection from the hot gases (the radiant component is assumed lost through the radiative fraction, usually assumed to be 30%) are neglected in the model.



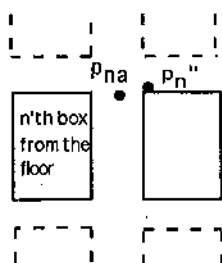
- 2) The temperature T_{nb} at the base of the box (defined in the figure below) is assumed to be raised to a constant temperature T_{na} over the height of the box.



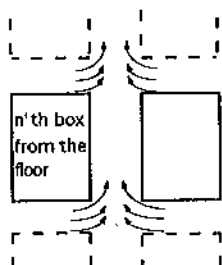
- 3) The static pressure p_{na} (defined in the figure below) at the centreline of the vertical flue and on the top of the rack storage, is equal to the hydrostatic pressure p outside the rack.



- 4) The static pressure p_{na} , at the centreline of the vertical flue and at the same height as the top of each intermediate box, is equal to the static pressure p_n'' on the top of each intermediate box in the intersecting horizontal flue (this is a description of the relationship between p_{na} and p_n'' in the figure below).



- 5) The air is assumed to be drawn through the horizontal flues due to pressure difference between inside and outside the rack. No air is assumed to "leak" out through the horizontal flues.



- 6) The cross sectional velocity and temperature distribution in the vertical flue is assumed to correspond to a "top hat" profile.

To determine the air flow inside the rack, various pressure drops are calculated. Subsequently, the mass flow rates inside the flues are obtained, which, in turn, give the corresponding gas temperatures (densities) and gas velocities. In assumption number 5) the model assumes that the air is assumed to be drawn through the horizontal flues due to pressure difference between inside and outside the rack. A lower pressure is created inside the rack. The pressure drops inside the rack are calculated by subtracting the pressure head changes due to entrance losses, obstructions (like the burner), changes in upward momentum of the heated air, wall friction, minor losses at intersections of horizontal and vertical flues and changes in density. In this report the model has been designed for 4 tiers but that can easily be extended to other tier heights.

A computer program, written in Fortran 77, has been developed to calculate the pressures and the flows within the rack. In Figure 3 a flow chart is shown to

explain the principal calculation procedure of the program developed. The program starts the calculations by "guessing" the mass flow rates followed by calculation of the pressure conditions. An iteration process is established at each tier until an overall pressure balance is obtained between the atmospheric pressure and the pressure inside the rack. The necessary equations to calculate the flow include the equations of continuity, energy and momentum.

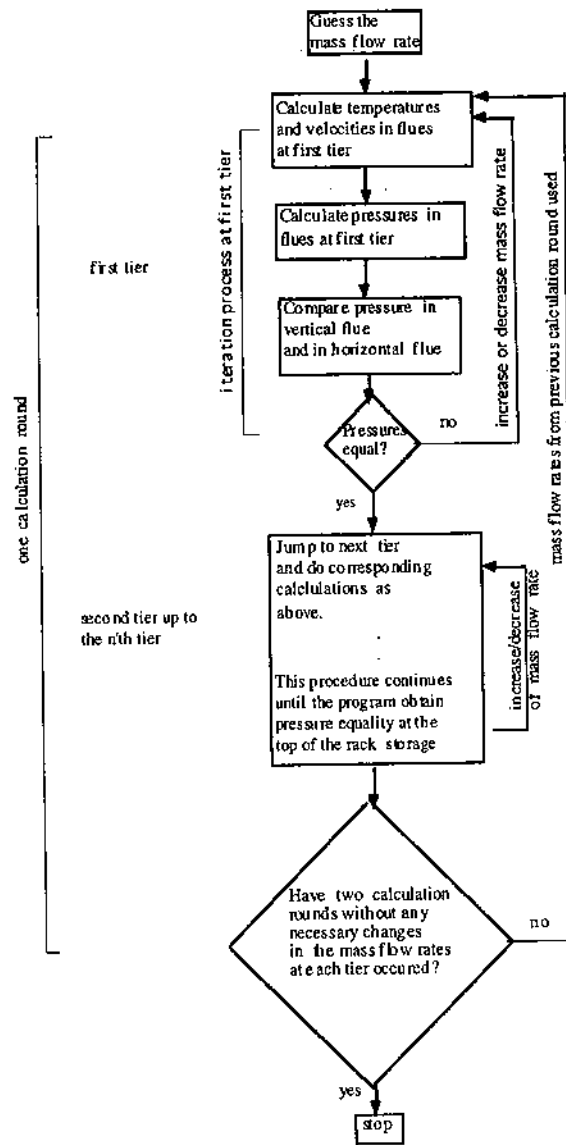


Figure 3 Flow chart showing the principal calculation procedure in the computer program developed.

As mentioned earlier, the program starts the calculation by "guessing" the mass flow rate and, based on that, the temperature and velocity can be determined. Knowing the temperature and the velocity, the pressure can be calculated. Equations to calculate these parameters are given in the following chapter.

3.1 The continuity equation

In Figure 4, the mass flow rates are defined for each flue. From continuity equation (conservation of the mass) and assumption number 5), i.e. no air is assumed to "leak" out through the horizontal flues, we find that

$$m_1 = 2m_{01} \quad (1)$$

$$m_2 = m_1 + 2m_{02} \quad (2)$$

$$m_n = m_{n-1} + 2m_{0n} \quad (3)$$

where n corresponds to the n 'th tier and m is the mass flow rate of air in the flues.

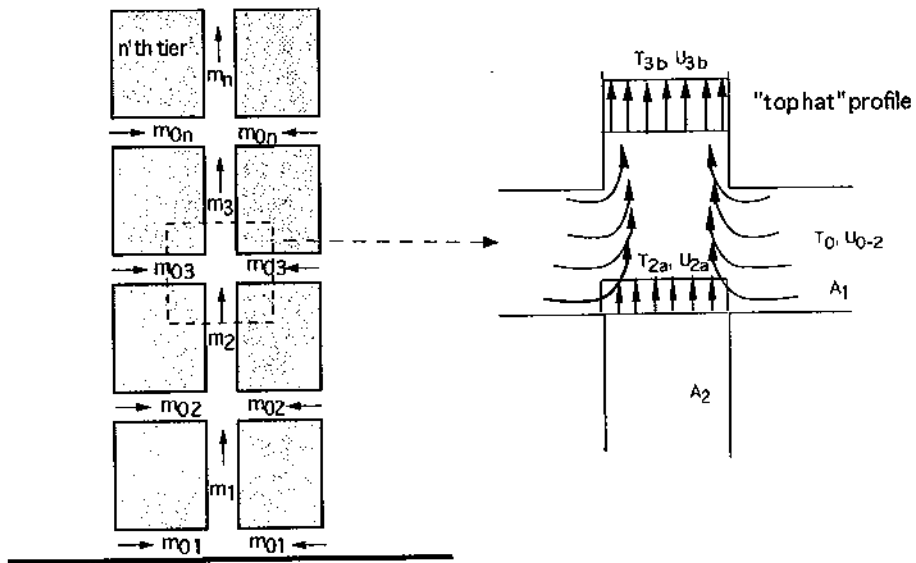


Figure 4 Definition of the mass flow rates in the vertical and horizontal flues. The framed part shows how the air is assumed to be drawn into the vertical flue.

3.2 The energy equation

When the mass flow rate in the vertical flue at each tier is known (the mass flow rate is constant between the base and the top of each box as this is a two dimensional case), the temperature at the corresponding height can be calculated according to the energy equation

$$Q_{c,na} = m_n C_p (T_{n,a} - T_o) \quad (4a)$$

$$Q_{c,nb} = m_n C_p (T_{n,b} - T_o) \quad (4b)$$

where

- $Q_{c,na}$ = accumulated convective heat release rate at the top of each box at tier number n , see Figure 5 (kW)
- $Q_{c,nb}$ = accumulated convective heat release rate at the base of each box at tier number n , see Figure 5 (kW)
- m_n = air mass flow rate at tier number n (kg/s)
- C_p = specific heat (kJ/kg K)
- $T_{n,a}$ = temperature at the top of each box at tier number n , see Figure 5 (K)
- $T_{n,b}$ = temperature at the base of each box at tier number n , see Figure 5 (K)
- T_0 = ambient temperature (K)

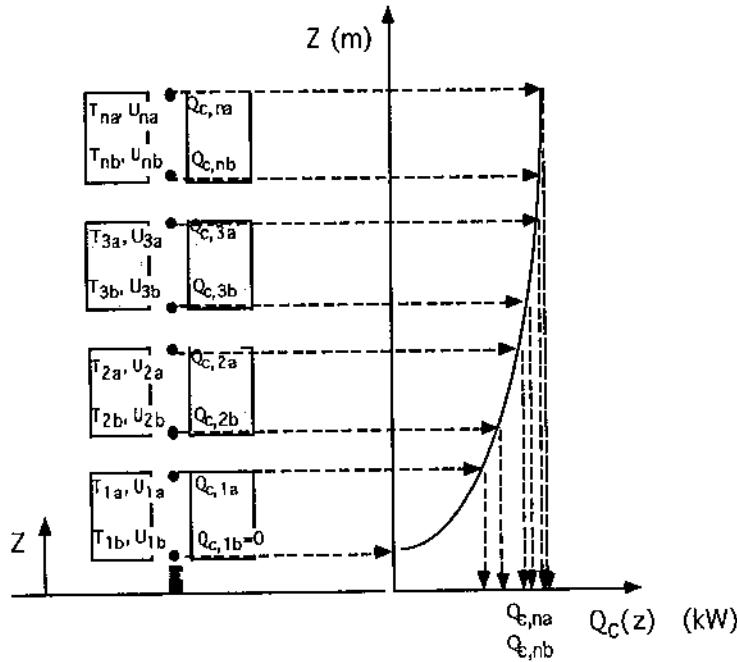


Figure 5 The model uses the convective heat energy at the lower and the upper part of each box. Knowing the mass flow rate at each tier the temperature and the velocity can be calculated at corresponding locations. At the lowest tier air at ambient temperature T_0 ($T_0 = T_{1b}$) enters the vertical flue and this air is assumed to be heated up to the temperature T_{1a} .

The convective heat energy, Q_c , used in equation (4), is the accumulated energy at each height. From an empirical distribution correlation based on measurements of the convective heat at each tier, the program determine the convective heat energy at the base and the top of each box (see Figure 5). The derivation of this correlation is described in Chapter 3.5. Accordingly, the temperatures at corresponding locations can be calculated from equation 5a and 5b.

$$T_{na} = T_o + \frac{Q_{c,na}}{m_n C_p} \tag{5a}$$

$$T_{nb} = T_o + \frac{Q_{c,nb}}{m_n C_p} \tag{5b}$$

Definitions of the temperatures are shown in Figure 5. From the relationship for mass flow rate ($m = \rho uA$) and the ideal gas law ($\rho T = \rho_0 T_0$) where influences of

pressure changes are neglected, velocity at the base and the top of each tier can be calculated by using equations 6a and 6b,

$$u_{nb} = \frac{m_n T_{nb}}{\rho_o T_o A_2} \quad (6a)$$

$$u_{na} = \frac{T_{na}}{T_{nb}} u_{nb} \quad (6b)$$

where

u_{na} =the velocity at the top of each box (m/s)

u_{nb} =the velocity at the base of each box (m/s)

A_2 =cross sectional area of the vertical flue space (m²)

3.3 Calculation of pressure drop

In Figure 6, the definitions of pressures and geometrical parameters are given. The pressure index (p_{1a} , p_{1b} , p_{2a} etc.) indicates the location of each point. For example, p_{1a} corresponds to the static pressure at top of the first box.

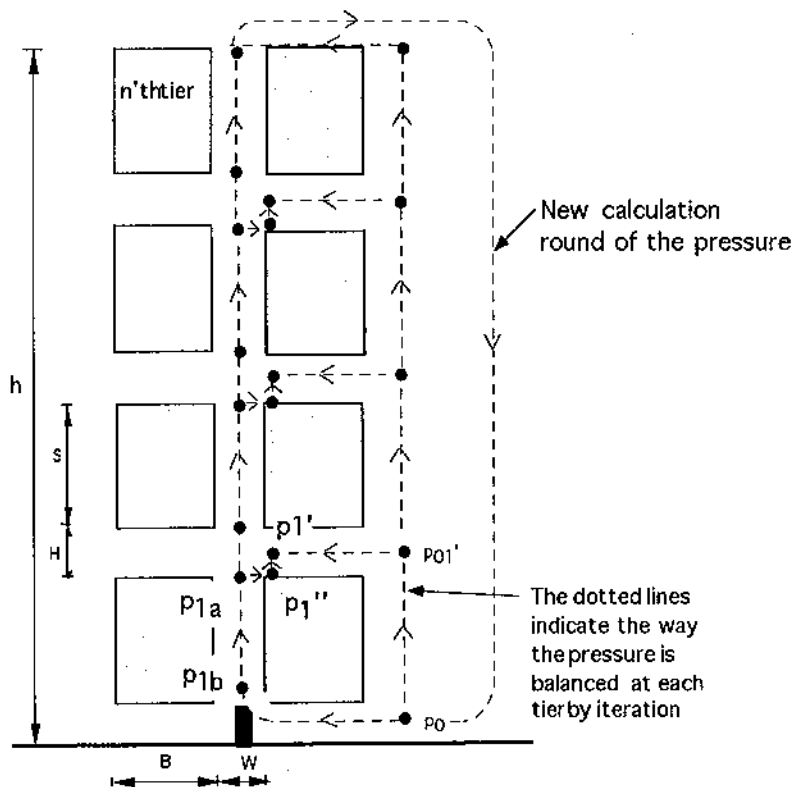


Figure 6 The definition of the pressures inside and outside the rack is shown in the figure. In the model the pressure is balanced at each tier by iteration. As an example, p_{1a} is assumed to be equal to $p_{1''}$. The pressure $p_{1''}$ is then "forced" by iteration to be equal to $p_{1'}$ plus the hydrostatic pressure difference between these points. This is done by changing the mass flow rate m_1 in each iteration step since the pressure p_{1a} changes when m_1 is changed. This process is carried out for the hole rack until a total balance in the system is obtained.

Assumption number 4 (see page 8) is very important as this assumption makes it possible to set up an iteration process to establish a pressure balance at each intersection and on the top of the rack. As an example, the pressure p_{1a} at the first tier is assumed to be equal to the pressure p_1'' , see Figure 6, and the pressure p_1'' is then "forced" by iteration to be equal to p_1' plus the hydrostatic pressure difference between these points. The pressure p_1' is obtained by calculating the head losses in the horizontal flue. In each iteration step the value of p_1'' is compared to the value of p_1' plus the hydrostatic pressure difference. Depending on whether the pressure p_1'' is higher or lower, the value of the mass flow rate m_1 (in the vertical flue at the first tier) is increased or reduced. A new value of p_1'' is obtained by changing the mass flow rate m_1 .

By aid of equations (5a,5b) and (6a,6b) (determination of temperature and velocity, respectively), where the mass flow rate and the convective energy are used as input, the pressures can be calculated from the equations developed in the following chapters. When a pressure balance is obtained at the top of the first tier the same procedure is carried out for the next tier above and then continued to the top of the rack. When a pressure balance is obtained at the top of the rack, after the first calculation round, the procedure is repeated for all tiers, starting at the lowest tier using the last obtained m_1 from the first iteration round, until an overall pressure balance for the rack is obtained.

3.3.1 Pressure drop at the first tier

In the following, equations to calculate the static pressure at the first tier (box) are developed. The static pressure p_{1b} (see Figure 7) can be obtained by using the modified Bernoulli equation between the base of the first box (just above the line gas burner) and the ambient air outside the rack.

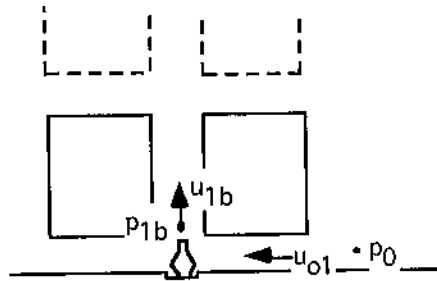


Figure 7 Definition of parameters used in equation (7).

The pressure drop in the horizontal inlet is then calculated in accordance to the following equation

$$\frac{p_{1b}}{\rho_0} = \frac{p_0}{\rho_0} - \frac{u_{o1}^2}{2} - h_{e0} - h_{f01} - h_{e1} \quad (7)$$

where h is a head loss per unit mass i.e.

$$h_{e0} = 0.5 \frac{u_{o1}^2}{2}$$

$$h_{f01} = f_D \frac{B}{D_{H1}} \frac{u_{o1}^2}{2}$$

$$h_{e1} = K_{11} \frac{u_{1b}^2}{2}$$

and where

p_0 = the hydrostatic pressure just above floor level, see Figure 6 (N/m²)

p_{1b} = the static pressure at the base of the first box, see Figure 6 (N/m²)

h_{e0} = the head loss at the entrance of the lowest horizontal inlet (N m/kg)

h_{f01} = the head loss due to friction inside the lowest horizontal inlet (N m/kg)

h_{e1} = the head loss due to the burner and change in direction of the flow (N m/kg)

ρ_0 = density at ambient temperature and pressure (kg/m³)

u_{01} = the velocity in the lowest horizontal flue (m/s)

u_{1b} = the velocity at the base of the lowest box (m/s)

f_D = the Darcy friction factor

B = width of the box (m)

D_{H1} = the hydraulic diameter of the horizontal flue (m)

K_{11} = the loss coefficient at the tee-intersection where the burner is located, see Figure 8.

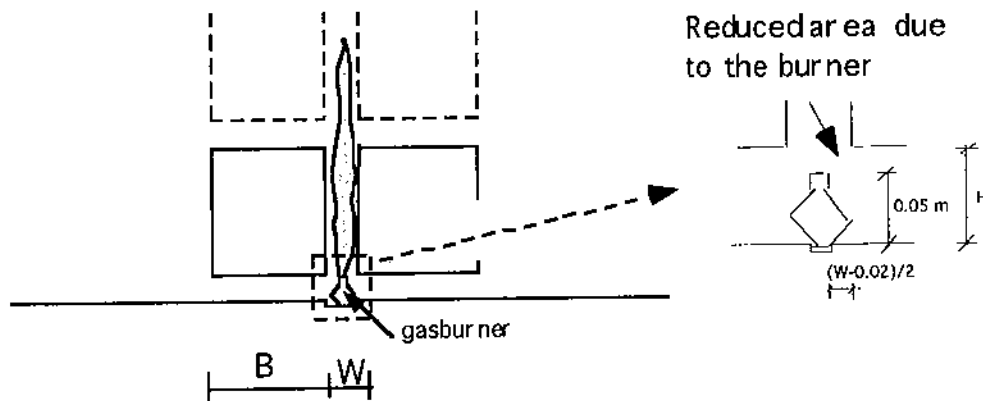


Figure 8 The loss coefficient K_{11} depends on the geometrical shape and location of the burner and the variation in W and H (see equation 8).

The loss coefficient K_{11} is very difficult to estimate and can only be determined accurately through laboratory tests. The value will depend on the geometrical shape and location of the burner and the variation of W and H . Such laboratory tests have not been performed and consequently the coefficient has been determined partly from the experiments and partly from handbook formulas.

The coefficient K_{11} is assumed to consist of an experimentally determined constant K_0 multiplied with a function $f\left(\frac{W}{H}\right)$ describing the influence of the cross-sectional ratio, $\frac{W}{H}$. Fried and Idelchik [17], p. 237, presents a relationship for a loss coefficient in a merging flow situation of a symmetrical (equilateral) wye with a sharp 90° turn without partition. Using that relationship and a volume flow ratio $\frac{1}{2}$ as in our case, the following relationship is obtained for K_{11} :

$$K_{11} = K_0 \left(1 + \frac{1}{4} \left(\frac{W}{H} \right)^2 \right) \quad (8)$$

K_0 in equation (8) has been experimentally determined and the best fit for all the cases was found to be 6.5.

The next step is to calculate the static pressure p_{1a} . The pressure can be obtained from a force balance on the gas volume (control volume) between the base and the top of the first box

$$p_{1b}WL - p_{1a}WL = m_1(u_{1a} - u_{1b}) + \frac{f_D}{4} \rho_{1a} P_s S \frac{u_{1a}^2}{2} + \rho_{1a} g WLS \quad (9)$$

where

P_s = the perimeter of the vertical flue (m)

S = the height of each box (m)

W = the width of the vertical flue (m)

L = the two dimensional length of the rack (m)

ρ_{1a} = the density of the heated gas in the vertical flue (\approx air) (kg/m^3)

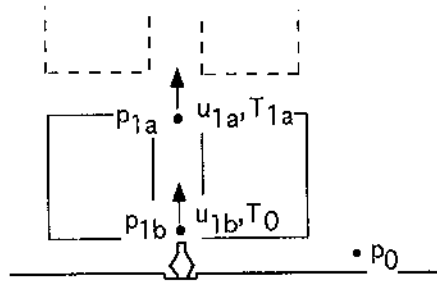


Figure 9 Definition of parameters used in equations (9) and (10).

The first term on the right hand side of equation (9) is due to change in momentum of the heated gas volume, the second term is due wall friction and the last term is due to gravity. The gas entering the base of first tier is at ambient temperature and for simplicity it is assumed that shortly after, due to a combustion process, the air is heated up to a uniform temperature T_{1a} over the height of the first box. Equation (9) can be rearranged to a form similar to equation (7)

$$\frac{p_{1a}}{\rho_0} = \frac{p_{1b}}{\rho_0} - \frac{T_0}{T_{1a}} \left(1 - \frac{T_0}{T_{1a}} \right) u_{1a}^2 - f_D \frac{T_0}{T_{1a}} \frac{S}{D_{H2}} \frac{u_{1a}^2}{2} - \frac{T_0}{T_{1a}} gS \quad (10)$$

by using relationships for the ideal gas law $\left(\rho_{1a} = \rho_0 \frac{T_0}{T_{1a}} \right)$, the mass flow rate

$(m_1 = \rho_{1a} u_{1a} WL)$ and the continuity $\left(u_{1b} = \frac{T_0}{T_{1a}} u_{1a} \right)$. D_{H2} is the hydraulic diameter

in the vertical flue and other definitions are given earlier in the text. To be able to

use equation (10), gas temperature and velocity must be known. This is obtained by "guessing" the mass flow rate m_1 and, by the aid of equations (5a, 5b) and (6a, 6b), the temperature and velocity are determined.

There are two ways to calculate p_1' (see Figure 10). Firstly, by using equation (10) and then the following equation which gives the hydrostatic pressure decrease between the top of the first box to the middle of the horizontal flue:

$$\frac{p_{1A}}{\rho_0} = \frac{p_{1B}}{\rho_0} - \frac{1}{2}gH \quad (11)$$

where H is the height of the horizontal flues in metre. Here, the index A for p_1' is used to distinguish it from the second way of calculate p_1' , namely

$$\frac{p_{1B}}{\rho_0} = \frac{p_0}{\rho_0} - 1.5 \frac{u_{02}^2}{2} - f_D \frac{B}{D_{H1}} \frac{u_{02}^2}{2} - g(S+H) \quad (12)$$

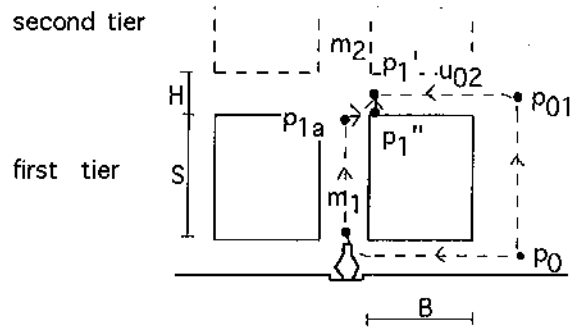


Figure 10 Definition of parameters used in equations (11) and (12). The dotted lines indicates the way the pressure calculation is carried out to obtain a pressure balance in the point where p_1' is defined.

Equation (12) represents a calculation of the head loss in the horizontal flue between the first and the second tier. The pressure is assumed to be balanced when the difference between the pressures p_{1A} and p_{1B} is equal to or less than 0.005 Pa. This was an arbitrarily chosen small value, but found to correspond to between 1 and 5 % of the pressure difference over the horizontal flue, $(p_1' - p_{01}')$. One could expect that the hydrostatic pressure difference in the horizontal flue, $(p_1' - p_{1B})$, would be much lower than the pressure difference over the horizontal flue, $(p_1' - p_{01}')$. However, calculations show that the pressure differences $(p_1' - p_{1B})$ and $(p_1' - p_{01}')$ are of the same order of magnitudes.

To be able to calculate p_{1B} the velocity u_{02} must be known. The velocity can be calculated from the mass flow rate m_{02} in the horizontal flue which is half the value of the difference between the mass flow m_2 at the second tier and the mass flow m_1 at the first tier (see equation 2 and Figures 4 and 10). In the first calculation round, the computer program assumes that the mass flow m_2 is 30 % higher than m_1 as the value of m_2 is not known at this stage. The value of 30 % was chosen arbitrarily but the average increase in the mass flow rate between the tiers is found to be of that order of magnitude. In the following calculation rounds, i.e. when the pressure has been balanced one time at all tiers, the program uses the mass flow rates obtained in the previous calculation round.

It was found that the pressure $p_1' B$ was not very sensitive to u_{02} as the flow is usually low (<0.4 m/s) in the horizontal flues. Consequently, the pressure calculations converged relatively quickly as $p_1' B$ did not change very much.

The friction factor f_D in equations (10) and (12) was calculated from the following expression

$$f_D = k_{non-c} \cdot 0.3164 Re^{-0.25} \quad (13)$$

where k_{non-c} is a correction factor due to other cross sections than circular. The value of 1.08, see Fried and Idelchik [17] diagram 2-6, was found to be the average value valid within the experimental range. The other part of equation (13) i.e., $0.3164 Re^{-0.25}$, is the friction factor for a smooth circular tube in a Reynolds number range of 4000 to 10^5 . Due to lack of exact knowledge about the surface roughness, the surface was assumed to be smooth. The Reynolds number was determined according to the following equation

$$Re = \frac{uD_{H1,2}}{0.956 \cdot 10^{-9} T^{1.7}} \quad (14)$$

where u is the flue velocity (m/s), $D_{H1,2}$ is the hydraulic diameter (m) for the horizontal flue and the vertical flue, respectively, and T is the corresponding gas temperature (K), i.e. T_{1a} at the first tier. The expression $0.956 \cdot 10^{-9} T^{1.7}$ in the denominator of equation (14) is a regression formula for kinematic viscosity based on tabulated data from [8]. Determination of the friction factor usually requires that the film temperature (in our case only in the vertical flue) is used for calculations of the Reynolds number. The film temperature is the average temperature of the wall temperature and the gas temperature. As the wall temperature is not known the calculated gas temperature was used. Calculations using wall temperatures varying from ambient to the gas temperature show that this assumption does not affect the results significantly. Accordingly, the computer program uses the calculated gas temperatures T_{na} in the vertical flues instead of the film temperature.

3.3.2 Pressure drop at intermediate tiers

The pressure calculations for the intermediate tiers (second and the third tier in our case) are identical. Accordingly, the following equations are applicable for both second and third tier. The pressure at the base of each intermediate box is obtained with the following equation which can be derived with aid of the modified Bernoulli equation between the two points shown in Figure 11.

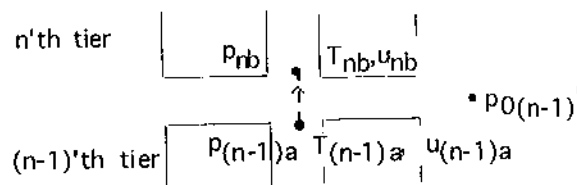


Figure 11 Definition of parameters used in equation (15) at an intersection between two tiers.

$$\frac{P_{nb}}{\rho_0} = \frac{P_{(n-1)a}}{\rho_0} + \frac{T_0}{T_{na}} \left(\frac{u_{(n-1)a}^2}{2} - \frac{u_{nb}^2}{2} \right) - \frac{T_0}{2} \left(\frac{1}{T_{(n-1)a}} + \frac{1}{T_{nb}} \right) gH - h_{en} \quad (15)$$

where

$$h_{en} = K_{ln} \frac{T_0}{T_{na}} \frac{u_{nb}^2}{2}$$

and

p_{nb} =the static pressure at the base of the n'th box (Pa)

u_{nb} =the velocity at the base of the n'th box (m/s)

T_{nb} =the gas temperature at the base of the n'th box (°C)

h_{en} =the head loss due to the converging flow at the intersection (N m/kg= m^2/s^2)

K_{ln} =the loss coefficient for the converging flow at the intersection

The second term on the right hand side of equation (15) originates from the "dynamic" head change. The third term relates to the average weight of the gas volume and the fourth term is due to the head loss at the intersection where horizontal inflow collide with upward moving flow in the vertical flue. The coefficient K_{ln} can be obtained from Table B-(6-36) in the ASHRAE handbook [9] for converging flows at an intersection. The coefficient depends on the ratio of the volume flows (m^3/s), Q_1 and Q_2 , between the tiers, see Figure 12.

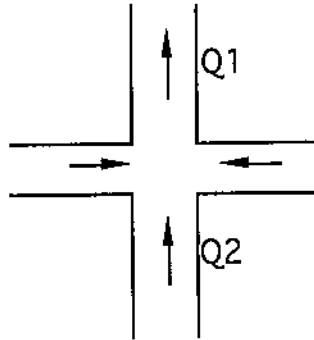


Figure 12 The figure shows converging flows at an intersection between two tiers. The loss coefficient for the main flow is determined from a table which require the ratio between the volume flows (Q_2/Q_1). The ratio is less than or equal to one.

The loss coefficient was determined from a regression formula made from the tabulated data (table 6-36) in the ASHRE handbook [9] ($K_{ln}=1.22-1.027(Q_2/Q_1)^{2.015}$).

The pressure at the top of each intermediate box can be obtained with aid of the following equation

$$\frac{P_{na}}{\rho_0} = \frac{P_{nb}}{\rho_0} - \frac{T_0}{T_{na}} \left(1 - \frac{T_0}{T_{na}} \right) u_{na}^2 - f_D \frac{T_0}{T_{na}} \frac{S}{D_{H2}} \frac{u_{na}^2}{2} - \frac{T_0}{T_{na}} gS \quad (16)$$

where n is the n'th tier, counted from the floor. This equation is identical to equation (10) and valid for all tiers (even the highest box).

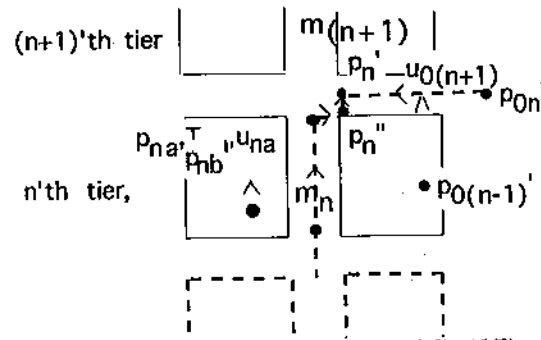


Figure 13 Definition of parameters used in equations (16), (17) and (18). The figure indicate as well the way the pressure is calculated to obtain pressure balance in p_n' .

Calculation of $p_n' B$ in the horizontal flue assumes that the program knows $m(n+1)$. Thus, in the first calculation round the program increases the value of m_n by 30% and that value becomes $m(n+1)$. The mass flow rate $m_{0(n+1)}$ in the horizontal flue is, by definition, half the difference between $m(n+1)$ and m_n . The velocity in the horizontal flue can be determined from $m_{0(n+1)}$. By using equation (17), which is identical to equation (12), the pressure $p_n' B$ can be determined

$$\frac{p_{nB}}{\rho_0} = \frac{p_0}{\rho_0} - 1.5 \frac{u_{0(n+1)}^2}{2} - f_D \frac{B}{D_{fl}} \frac{u_{0(n+1)}^2}{2} - gn(S + H) \quad (17)$$

The pressure $p_n' A$ is obtained from equation (18), which is identical to equation (11)

$$\frac{p_{nA}}{\rho_0} = \frac{p_{na}}{\rho_0} - \frac{1}{2} gH \quad (18)$$

The indices A and B in equations (17) and (18) indicate the two different ways of calculating the pressure. When the pressures have been balanced the difference between the pressures $p_n' A$ and $p_n' B$ is equal to or less than 0.005 Pa and the program continues to the highest tier (the fourth tier in our case).

3.3.3 Pressure drop at the highest tier

First the program determines the pressure p_{4b} at the base of the fourth box from equation (15) ($n=4$).

The coefficient K_{14} is determined from a regression formula given on page 18. The temperatures and velocities, used in equation (15), are obtained with aid of equations (5a, 5b) and (6a, 6b) where the mass flow rate and the convective heat output are used as input. The program starts the calculations at the fourth tier by putting m_4 , i.e. the mass flow at the fourth tier, equal to the latest used value of m_3 , increased by 30 %. Fractions of the total convective heat energy are determined at the base and the top of the fourth box (see Figure 5) in accordance to the distribution model described in chapter 3.5.

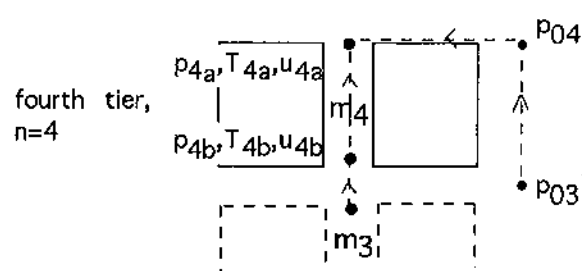


Figure 14 Definition of parameters used in equations (15) and (19) where $n=4$ The figure indicate as well the way the pressure is calculated to obtain pressure balance in p_{4a} .

Then the pressure p_{4a} at the top of the fourth box is determined from equation (16) ($n=4$). The fourth tier is the highest tier, which means that the pressure p_{4a} is (according to assumption number 3 on page 8) assumed to be equal to the static pressure outside the rack at the corresponding height. This means that the pressure p_{4a} can be balanced in accordance to following equation

$$\frac{p_{na}}{\rho_0} = \frac{p_0}{\rho_0} - g(n(S + H) - \frac{1}{2}H) \quad (19)$$

where $n=4$. When the equations have been balanced the difference is equal to or less than 0.005 Pa.

3.3.4 Pressure calculations after the first round

When the program has run through all tiers, a new calculation round is started by calculating the pressure at the lowest tier again (see Figure 6). The program applies the latest used mass flow rates from the previous calculation round. Iterations for individual tiers are repeated until an overall pressure balance is obtained, i.e. it is not necessary to change the mass flow rates at each tier between calculation rounds. When the program have run twice through the rack without any changes in the mass flow rates, the program stops. At this stage all mass flow rates, temperatures and velocities in the flues are known. Comparison of calculated results and experiments are presented in Chapter 5.

3.4 The flame height

In the following a simple model is proposed to calculate the flame height in the vertical flue. This is necessary to be able to determine the fractions of the total convective heat energy at the top and the base of each box. The flame height is determined by simply comparing the amount of available air and fuel at each tier. It is assumed that the flame tip will extend to a height where the total flux of air entrained is sufficient to complete the combustion reactions. For open buoyancy-controlled diffusion flames Heskestad [10] assumed the air demand from the surroundings to be proportional to the stoichiometric requirements of the pyrolysis gases

$$m_e \propto m_f r \quad (20)$$

where m_e is the total mass-entrainment rate of air below the level of the flame tip, m_f is the pyrolysis or mass burning rate and r is the stoichiometric mass ratio, air to volatiles. The proportionality constant will be greater than unity, because much of the air entrained in the vertical flues never takes part in the combustion reactions. The following equation defines the air-to-fuel stoichiometric fraction [11,12] or the "equivalence ratio" as defined in [2]

$$\phi = \frac{m_e}{m_f r} \quad (21)$$

For open diffusion flames, as in the case of natural fires, complete combustion usually cannot be achieved at $\phi=1$ [12]. For turbulent diffusion flames in rack storage the value of ϕ has been empirically determined in the first phase of the project, see Ingason [1]. From regression curves on the experimental data the value for ϕ was found to be 6 at the flame tip for $W=50$ mm, $\phi=7.6$ for $W=75$ mm and $\phi=10$ for $W=100$ mm. The value of ϕ was determined from the experimental data [1] by using equation (21) and (22). Regression of all data points yield $\phi=7.5$ at the flame tip [1]. According to Delichatsios [13], ϕ can be as much as 10 for free-burning buoyant turbulent diffusion flames (based on measurements presented in [14,15]). There are two major differences in the present study compared to earlier studies [11,12,13,14], namely, the air is entrained stepwise (through the horizontal flues) and the flow conditions are controlled by solid boundaries (walls). We assume, as for open flames, that there is a direct relationship between entrained air and flame heights.

At each tier the mass flow rate m_e is compared to the amount of mass burning rate m_f . The mass burning rate m_f is found from equation (22),

$$m_f = \frac{Q}{\Delta H_c} \quad (22)$$

where Q is the total heat release rate and ΔH_c is the heat of combustion per unit mass of the fuel. The mass flow rate in the flues is calculated by using the convective heat release rate Q_c . Heskestad and Yu [2] found that the difference between Q and Q_c was about 30 % within the stack they used. Measurements presented by Ingason [5] for almost an identical experimental set-up as modelled here show that there is a 30 % difference between Q and Q_c measured above the rack by a hood system. Thus we have a fairly good reason to assume that $Q_c=0.7 Q$.

There are two steps taken to determine the flame height. First we determine at which tier (flame height interval) the flames (L_{fn}) will extend by comparing the calculated mass flow rates and the fuel flow rates. This is done in accordance to the following conditions:

nr)	<u>Conditions</u>	=>	<u>Flame height interval</u>
1)	$m_f < m_1/r\phi$;		$L_{f1} < 1.5H+S$
2)	$m_1/r\phi < m_f < m_2/r\phi$;		$1.5H+S < L_{f2} < 2.5H+2S$
3)	$m_2/r\phi < m_f < m_3/r\phi$;		$2.5H+2S < L_{f3} < 3.5H+3S$
4)	$m_3/r\phi < m_f < m_4/r\phi$;		$3.5H+3S < L_{f4} < 4H+4S$
5)	$m_f > m_4/r\phi$;		$L_{f5} = 4H+4S$

For example if the fuel flow rate m_f is greater than the mass flow rate m_1 divided by $r\phi$ but less than the mass flow rate m_2 divided by $r\phi$, the flame height will be greater than $(1.5H+S)$ and less than $(2.5H+2S)$. The next step is to determine how far the flames will extend within this interval. We simply assume that the flames will extend proportional to the ratio of available fuel and air. This assumption can be justified [1] where it was found that the heat output Q tended to be linearly proportional to the flame height L_f . Thus, for the n 'th tier satisfying the conditions given above the following equation is used to calculate the flame extension within the interval

$$L_{fn} = S_{n-1} + (S_n - S_{n-1}) \frac{r\phi m_f - m_{n-1}}{m_n - m_{n-1}} \quad (23)$$

S_n and L_{fn} for each tier are defined in Figure 15. The flame height is not calculated above the rack storage (condition nr 5). It is simply put equal to the rack storage height $(4H+4S)$. In the model, determination of mass flow rates and flame height is dependent on each other but these parameters will finally converge when the pressures have been balanced. The conditions necessary to determine the flame height at respective elevations are shown in Figure 15.

To better explain this procedure we give an example:

Assume a heat release rate $Q=20$ kW, ΔH_c and r for propane 46.45 kJ/g and 15.7, respectively, and $\phi=7.5$, $W=50$ mm and $H=50$ mm. From equation (22) we get $m_f=0.4306$ g/s. Calculations yields the following mass flow rates: $m_1=0.0184$, $m_2=0.0384$, $m_3=0.0504$ and $m_4=0.0588$ kg/s. Accordingly, we can calculate the following ratios: $m_1/r\phi=0.156$ g/s, $m_2/r\phi=0.326$ g/s, $m_3/r\phi=0.428$ g/s and $m_4/r\phi=0.500$ g/s. Thus, the flame height will be greater than $S_3=0.88$ m and less than $S_4=1.14$ m (see Figure 15) since $0.428 < 0.4306 < 0.500$, i.e. we use condition

nr. 4. The next step is to more accurately determine the flame height ($r\phi m_f=0.0507$):

$$L_{f4} = 0.88 + (1.14 - 0.88) \left(\frac{0.0507 - 0.0504}{0.0588 - 0.0504} \right) = 0.89m$$

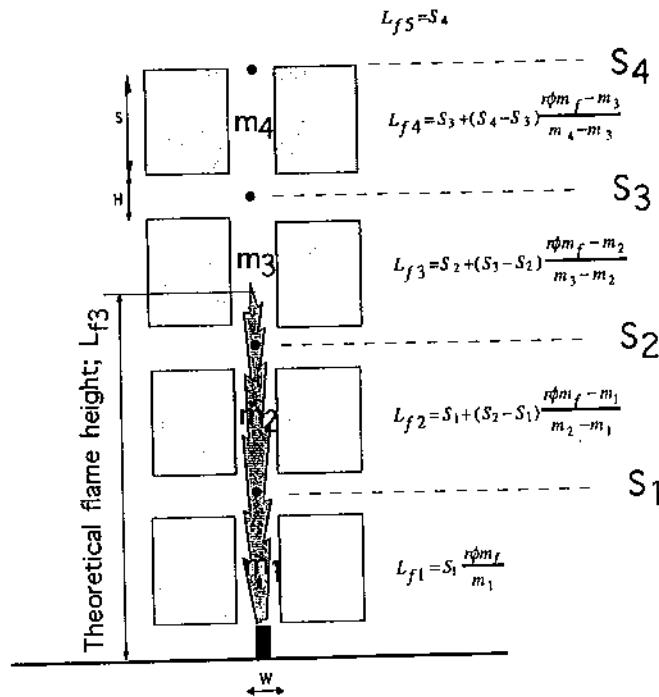


Figure 15 A simple theoretical model was used to calculate the flame height. By simply compare the amount of available air and fuel at each tier the flame height is determined.

3.5 Distribution of the convective heat energy

It is known from measurements with free-burning diffusion flames [7] that the fractions of the total heat released increases with the flame height. Here, we assume that close to the burner no energy has been released and at the flame tip all energy has been released. The distribution of the convective heat energy between the flame tip and the burner needs to be determined from experiments.

This has been done by calculating the experimental convective heat release rate $Q_{c,exp}$ with aid of the measurements presented in [1]. From equation (4), $Q_c = m C_p \Delta T$; assuming $C_p = 1000 \text{ J/kg } ^\circ\text{C}$, the $Q_{c,exp}$ was determined. The mass flow rate was calculated on the basis of a single point measurement at the flue centreline and not on an integrated value over the cross section (averaged value) which would have been better. Due to disturbance and creation of turbulent eddies at the interactions between the tiers, the flow profiles are very difficult to predict. Therefore it was decided to simply use the measured value and assume the temperature and velocity to be uniform over the cross section. In Figure 16, a plot of z/L_f versus $Q_{c,exp}/Q$ is shown, where $Q_{c,exp}$ is the calculated value at the height z , Q is the total heat release rate from the burner and L_f is the observed flame height [1] (averaged value of the fluctuating visible flame tip). These observations

were somewhat subjective as the boxes mostly concealed the visible flame tip. The accuracy of these observations was deemed to be approximately ± 50 mm.

One could expect the ratio $Q_{c,exp}/Q$ at the flame tip ($z/L_f=1$) to be close to 0.7. Apparently this is not the case, and the reason is probably the flue width dependence of the flow profiles and thus the calculated mass flow rates. However, by putting the ratio $Q_{c,exp}/Q$ equal to one at $z/L_f=1$ (and thereby raising the entire curve in the same proportion) we can use this diagram as a form curve $r(z/L_f)$, see equation (24), to determine the heat fraction along the flame height.

$$r\left(\frac{z}{L_f}\right) = 1.0373 \left(1.004 - 0.04 \left(\frac{z}{L_f} \right)^{-1.571} \right) \quad (24)$$

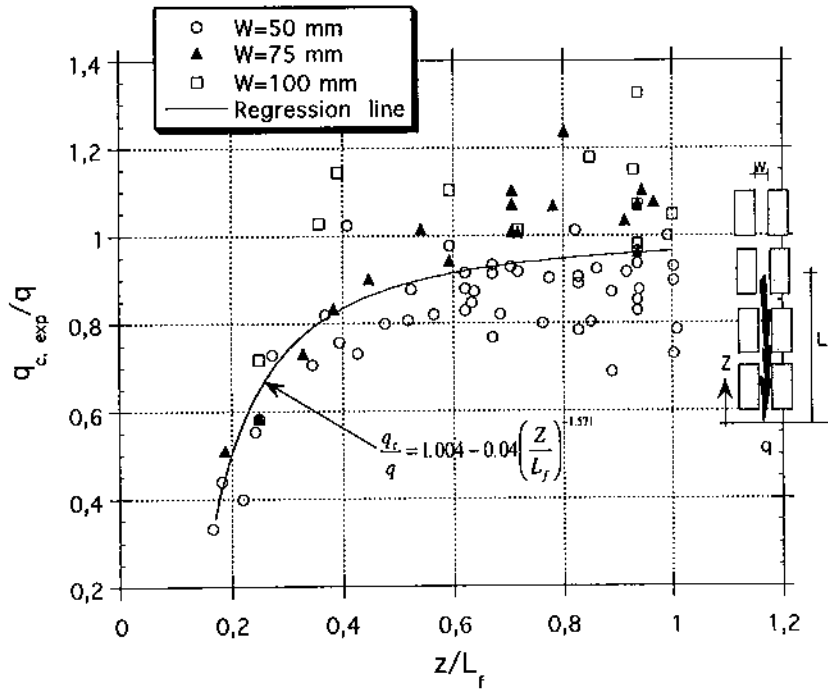


Figure 16 A plot of $Q_{c,exp}/Q$ versus z/L_f is shown where $Q_{c,exp}$ is the calculated value at the height z , Q is the total heat release rate from the burner and L_f is the observed flame height (averaged value of the fluctuating visible flame).

The Q_c at the base and the top of each box is then determined in accordance to the following equation

$$Q_c = 0.7Qr(z/L_f) \quad (25)$$

where $0.7Q$ is assumed to be the total convective heat from the burner and $r(z/L_f)$ is obtained from equation (24). L_f is determined in accordance to Chapter 3.4.

4 Experimental set-up

A brief description of the experimental set-up is given here while a more thorough description is given by Ingason [1]. The following combinations of parameters were used;

W=50 mm, 75 mm, 100 mm with H=50 mm

W=50 mm with H=75 mm

W=50 mm with H=100 mm

where W is the width of the vertical flue and H the height of the horizontal flue.

The following four heat release rates were used for each of the combinations above;

Q=18.84 kW, 24.8 kW, 34.7 kW and 44.5 kW

The rack storage consisted of rectangular Navilite N boxes, 0.59 m long, 0.235 m high and 0.22 wide, held up by two narrow steel columns. The rack storage was two boxes wide and four boxes high (see Figure 1). Walls were put at each end of the boxes to create two dimensional conditions. Especially made wings were mounted at each wall in order to minimise the boundary effects of the air flowing in through the horizontal flues (see the plan view in Figure 1). The Navilite N plates used to build the boxes were 9.5 mm thick and the thermal data for the Navilite N is, heat conductivity 0.12 W/m °C, specific heat 800 kJ/kg and density 700-780 kg/m³.

The length of the gas burner was 590 mm and other dimensions of the gas burner are given in [1].

Prior to the tests, the line burner was calibrated for the heat outputs used in the test series [1]. During the test series the different heat outputs were manually adjusted by a rotameter. It has been shown [5] that putting the line burner inside the rack does not affect the total heat release rate compared to free burning. As this test set-up is very similar to the one presented in [5] it was thought unnecessary to measure the heat release rate from each test.

The instrumentation consisted of type K thermocouples (0.25 mm) and bi-directional probes (D=16 mm and L=32 mm) located at the centreline in the vertical flue at different heights. In Figure 17 the instrumentation layout is shown. To avoid influence of the bi-directional probes on each other they were mounted in a staggered pattern.

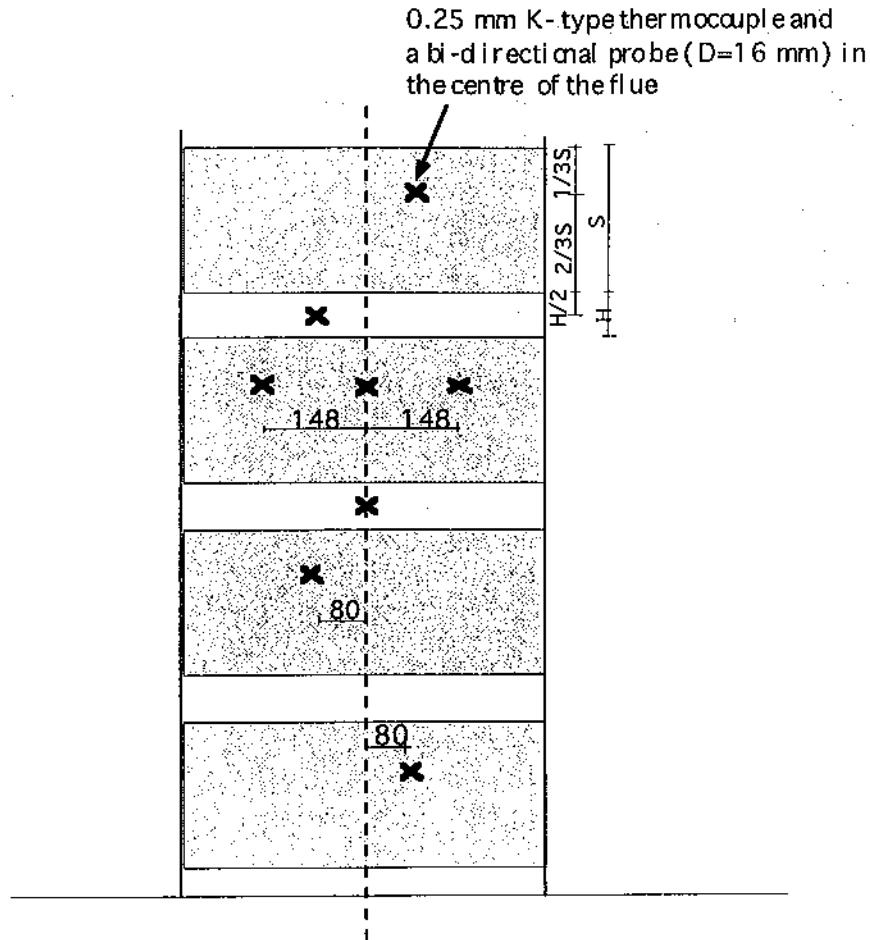


Figure 17 The figure shows the layout of the instruments used. The instrumentation consisted of thermocouples and bi-directional probes located at the centreline of the flue. The vertical distances to the measuring probes are given as fractions of S (0.235 m) and H (50, 75, 100 mm), respectively. The location of the probes is identical for the other tiers. All dimensions are in mm.

The relationship between pressure and velocity includes corrections for variation in the Reynolds number according to calibration curves reported by McCaffrey and Heskestad [16]. The results were averaged over the time interval during which the measured gas temperatures and velocities were reasonably steady. It was found that this time was about four minutes, i.e. the last four of the six minutes of the test. In the beginning of a test, the walls were relatively cold, causing large heat losses. After about 2 minutes the gas temperature was found to increase moderately until the end of the test. The temperatures were corrected due to radiation effects. In [5] a formula for the correction of a 0.25 mm thermocouple is given.

5 Results

In the following, calculations are compared to experimental results. First, calculation of mass flow rates at different tiers are compared to experimental results for different flue widths. Furthermore, flame height, temperature and velocity measurements are compared to calculated values.

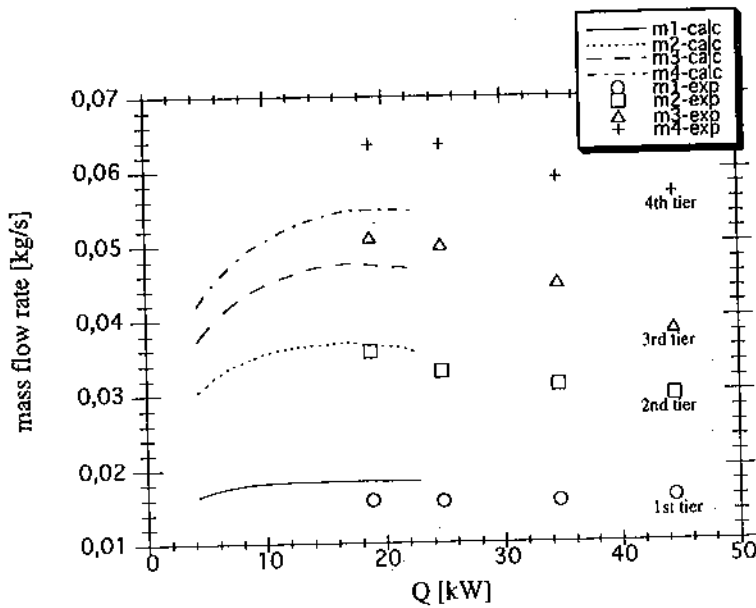


Figure 18 Comparison between calculated and measured mass flow rates at each tier in the two dimensional rack storage, $W=50$ mm and $H=50$ mm. The calculated values are only presented when the flame height is theoretically lower than the rack storage.

Figure 18 shows that the agreement between calculated mass flow rate and measured ones is reasonably good at the lower tiers but poor at the higher tiers. No considerations have been given to possible influences of high aspect ratios (L/W) on the K_{In} values, i.e. aspect ratios $L/W=6-12$ in our case. One could expect that the values of K_{In} will become lower for higher aspect ratios. In Fried and Idelchik [17] the influences of high aspect ratios are shown for rectangular elbows (p. 168-169). The loss coefficient will decrease by about 25-30% for aspect ratios 5-8 compared to aspect ratio equal to one. If we assume that a similar relationship exists for converging flows at an intersection we can reduce the calculated aspect ratios by a certain value. It is found that 25 % reduction yields a reasonable good agreement with the experimental data for $W=50$ mm and $H=50$ mm. In Figure 19, we have used 25 % reduction on the K_{In} values obtained from the correlation given on page 18.

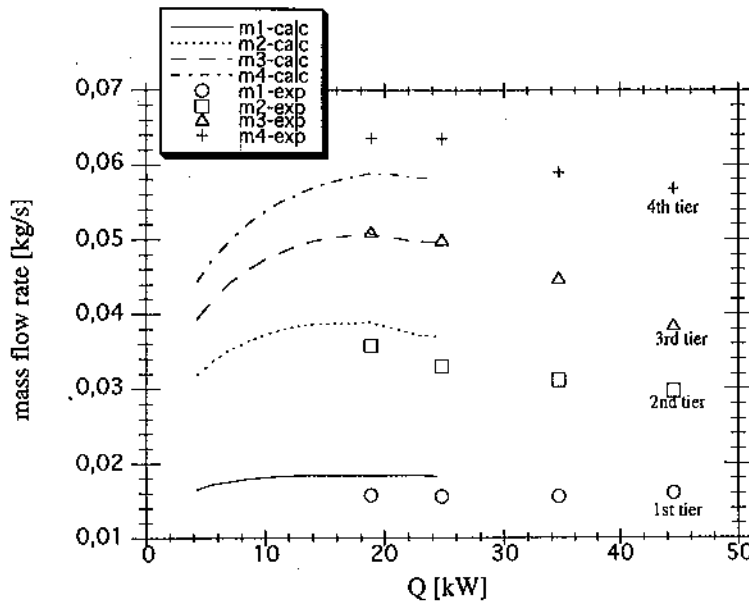


Figure 19 Comparison of calculated and measured mass flow rates at different tiers for $W=50$ mm and $H=50$ mm. Observe that calculated mass flow rates are only shown for those cases where the calculated flame height is lower than the height of the rack storage.

Clearly the results in Figure 19 are improved compared to Figure 18 at the two highest tiers, but deteriorate slightly at the second tier. The difference between the mass flow rates is increased slightly and the curves are moved upwards. In general it is found that the calculated mass flow rates tend to be slightly higher than the measured ones at the second tier, about the same at the third tier and slightly lower at the fourth tier. The effects of heat losses to the walls have not been considered in the model (assumption number 1 at page 7) but rough calculations indicate that if heat losses are introduced the mass flow rates will be increased slightly, especially at the higher tiers.

It is interesting to observe that the mass flow rate at each tier tends to be nearly constant for heat outputs greater than 15-20 kW. The reason for this has been given by Ingason [1] for a single stack, and is clearly valid for the individual tiers as well. This means that the forces dominating the flow at each tier are about the same as for a single stack.

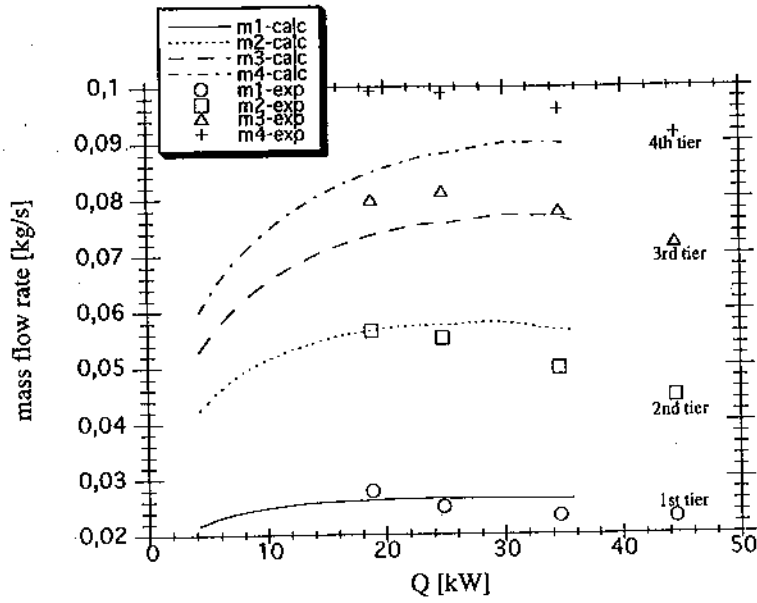


Figure 20 Comparison between calculated and measured mass flow rates at different tiers for $W=75$ mm and $H=50$ mm.

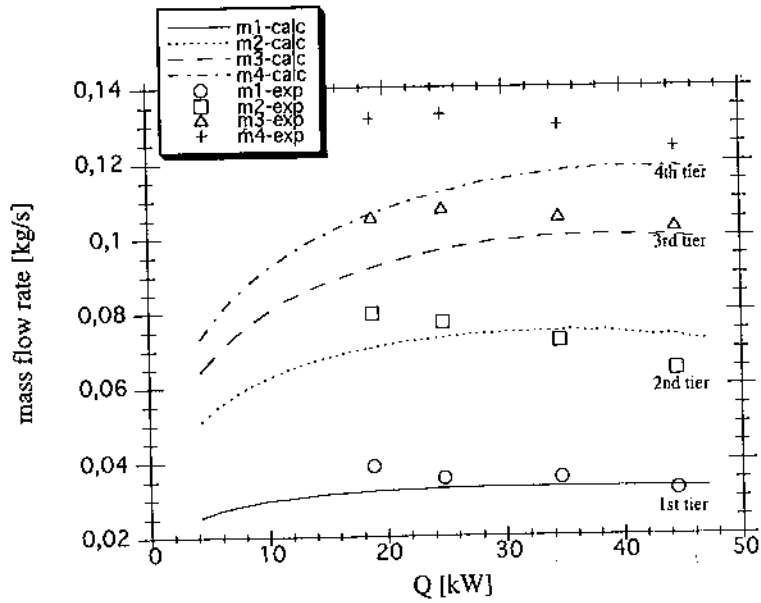


Figure 21 Comparison between calculated and measured mass flow rates at different tiers for $W=100$ mm and $H=50$ mm.

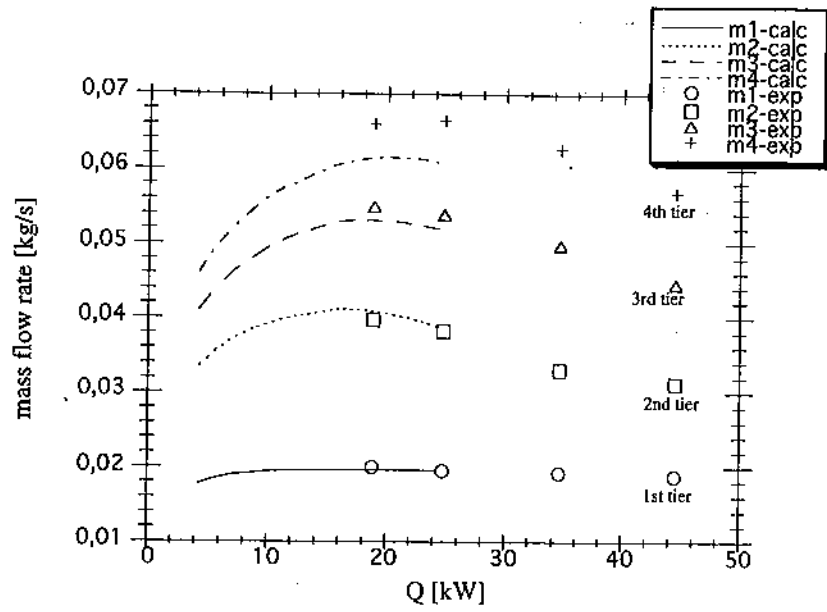


Figure 22 Comparison between calculated and measured mass flow rates at different tiers for $W=50$ mm and $H=75$ mm.

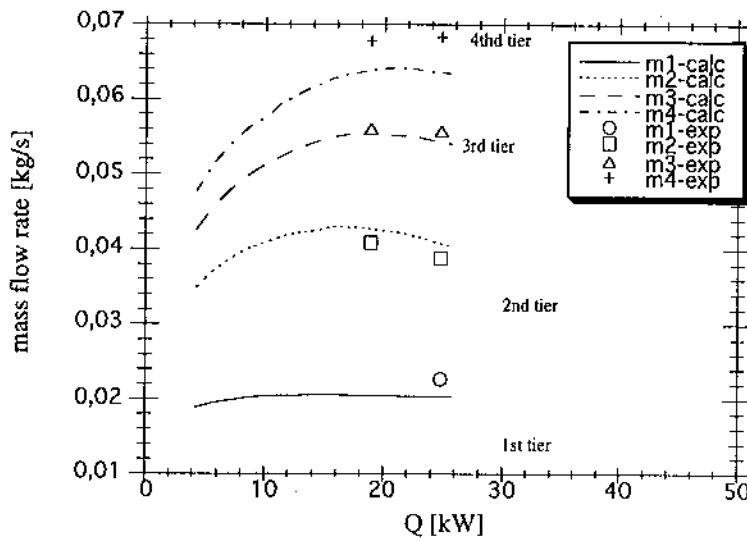


Figure 23 Comparison between calculated and measured mass flow rates at different tiers for $W=50$ mm and $H=100$ mm.

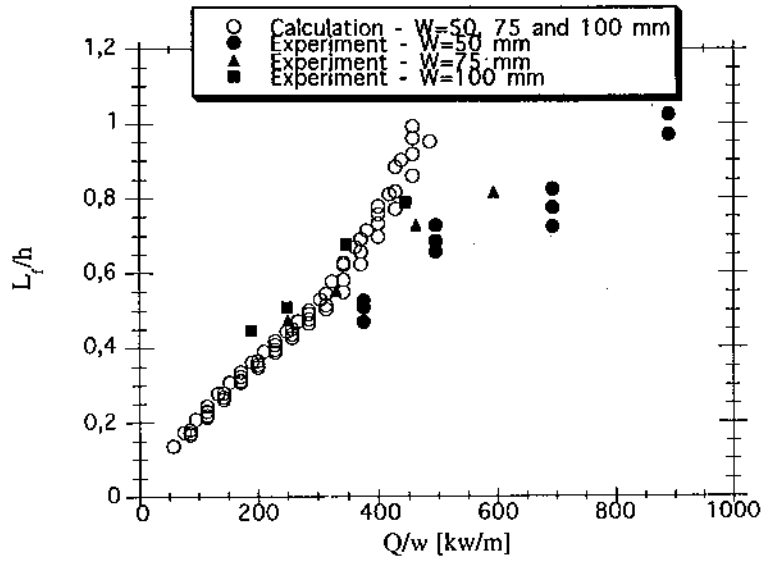


Figure 24 Comparison between observed and calculated flame heights. The agreement is less good at higher tiers. The mass flow rates at the higher tiers are underestimated and consequently the flame heights become higher.

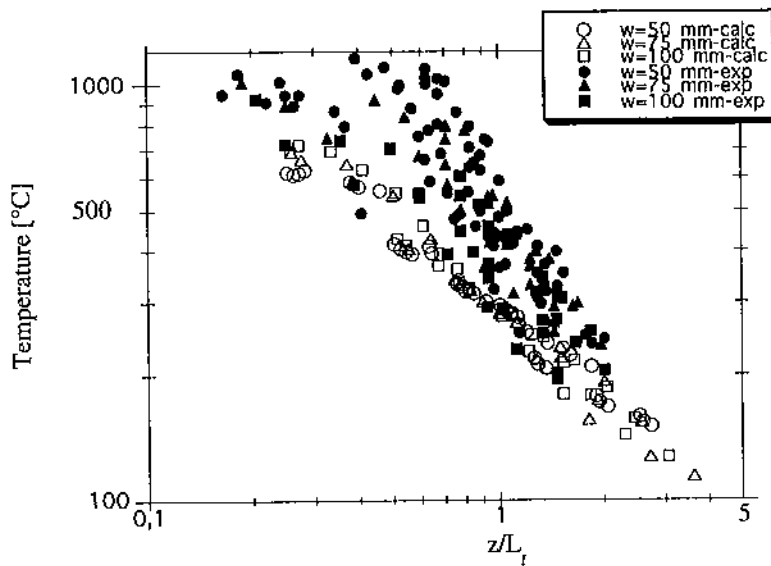


Figure 25 Comparison between measured centreline temperature and the calculated (average) temperature.

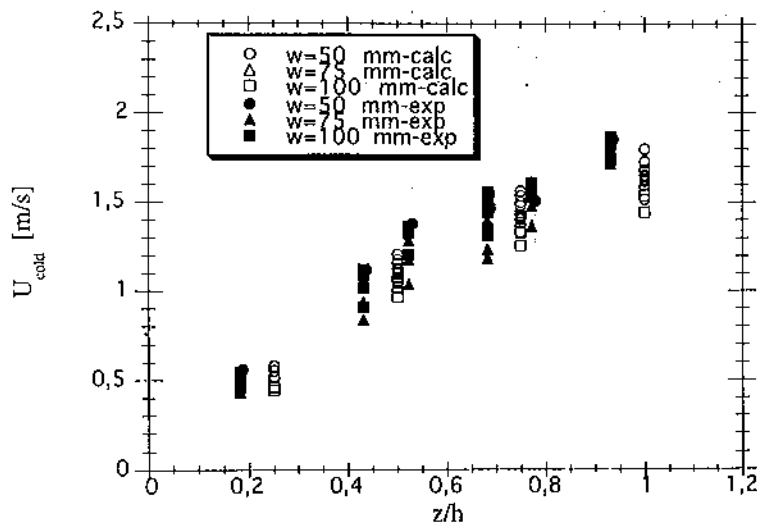


Figure 26 Comparison between "cold"-velocity based on measurements and on calculation.

Comparison between calculated and observed flame heights in Figure 24 are reasonable good at the lower tiers but not at the higher tiers. Further it can be observed that the slope of the theoretically obtained curve differs considerably from the experiments, especially at the higher tiers. This may be explained in the following way: the mass flow rates at the higher tiers are underestimated and consequently the flame heights become higher than the experimentally obtained. The slope of the curve may change slightly if the mass flow rates are increased at the higher tiers. This can be demonstrated by the following example: we assume $Q=23$ kw, $W=50$ mm, $H=50$ mm, $h=1.14$ m, $\phi = 7.5$, $m_4=0.058$ kg/s and $m_3=0.050$ kg/s. Thus by using equations (21),(22) and (23) we find $L_f/h=1$ and $Q/W=460$ kW/m. If we instead use the experimentally obtained mass flow rates we obtain $L_f/h=0.9$ at $Q/W=460$ kW/m. The slope of the curve in Figure 24 is thus decreased slightly.

Furthermore, the influence of using a constant value of ϕ may affect the results considerably. An average value of 7.5 for all three flue widths was used in the calculations whereas we know it can vary from 5 - 12 depending on the flue width [1]. From [1] we know the average ϕ value for $W=50$ mm is 6. To demonstrate the effects of varying ϕ we can continue with the example given above. If we use $\phi =6$ instead of 7.5 we will obtain $L_f/h=0.71$ at $Q/W=460$ kW/m instead of $L_f/h=1$. This is in line with the experimentally obtained data points. Thus, the results of the flame height model may be improved by using ϕ as a function of the width. Actually the experimental data given in Figure 24 indicate that there is a flue width dependence of the flame height and thus of ϕ .

In Figure 25 the calculated temperature is found to be considerably lower than the experimental values below the flame tip ($z/L_f=1$). Since the flame height model predicts L_f poorly, especially at the higher tiers, a direct comparison is difficult to make.

In Figure 26 we see about the same values of "cold"-velocity for the experimental and calculated values. The "cold"-velocity is defined as $u_{cold} = u \frac{T_0}{T}$ where u is the measured velocity.

6 Conclusions

A theoretical model to predict mass flow rate, temperature, velocity and flame height in a two dimensional rack storage was developed. It was necessary to introduce generalized empirical corrections of loss coefficients, stoichiometric requirements, and distribution of heat release in the model. Comparison of calculated and measured values show that the dominating flow mechanisms are accounted for in the model.

The model shows that the air flows into the horizontal flues due to the pressure difference between inside and outside of the rack storage. According to the results the leakage out through the horizontal flues is probably very small, if any. It is found that about one third of the air enters through the lowest flue. The model predicts very well what was observed in [1] that the height of the horizontal flues have insignificant effects on the flow inside the rack storage, whereas the width of the vertical flue dominates the flow.

The model is found to predict the flame heights poorly in the upper part of the stack. The flame height model needs to be improved. By adding heat losses the mass flow rates at higher levels will increase and the slope of the curve will thus be reduced. Furthermore, by using an equivalence ratio ϕ as a function of the flue width will also improve the results. The flame height model is found to be very sensitive to the value of ϕ . It is proposed to use CFD (Computational Fluid Dynamics) calculations in the continuing work. Thus the flue width dependence of the experimentally obtained mass flow rates and of ϕ can be investigated.

The calculated temperature is found to be considerably lower than the experimental values below the flame tip.

The so called "cold"-velocity, $u_{cold} = u \frac{T_0}{T}$, agrees reasonable well with the experimental data. The cold velocity is nearly linearly increasing below half the stack height whereas the increase is found to decay slightly above half the stack height.

7 Acknowledgement

The project was sponsored by the Swedish Research Board (BRANDFORSK) which is gratefully acknowledged. A co-operation between Lund University (LTH) and SP was established at early stage of the project. Special thanks to my supervisor at LTH, Dr. Göran Holmstedt and Dr. Bror Persson at SP for their valuable comments. The author stayed three months at Factory Mutual Research Corporation (FMRC) working on the theoretical model presented in this report under supervision of Dr. Gunnar Heskestad. He is gratefully acknowledged as well as his colleagues Dr's. J. De Ris, H-Z Yu, S. Nam and M.A. Delichatsios for their encouragement and help in developing this model. Special thanks to Mr. Cheng Yao and his personnel who made my stay so enjoyable at FMRC.

8 Nomenclature

A_2	cross sectional area of the vertical flue space (m^2)
B	width of the box (m)
C_p	specific heat (kJ/kg K)
D_{H1}	the hydraulic diameter of the horizontal flue (m)
D_{H2}	the hydraulic diameter of the vertical flue (m)
E	height of the burner (m)
f_D	the Darcy friction factor
g	acceleration of gravity (m/s^2)
H	height of the horizontal flues (m)
ΔH_c	heat of combustion per unit mass of the fuel (J/kg)
h_{e0}	head loss at the entrance of the lowest horizontal inlet ($Nm/kg=m^2/s^2$)
h_{f01}	head loss due to friction inside the lowest horizontal inlet (Nm/kg)
h_{e1}	head loss due to the burner and change in direction of the flow (Nm/kg)
h_{en}	head loss due to the converging flow at the n'th intersection (Nm/kg)
K_{11}	loss coefficient at the tee-intersection where the burner is located
K_{1n}	loss coefficient for the converging flow at the n'th intersection
L	longitudinal length of the rack
L_f	flame height (m)
m_n	mass flow rate in the vertical flue at the n'th tier (kg/s)
m_{0n}	mass flow rate in the horizontal flue at the n'th tier (kg/s)
m_f	fuel flow (kg/s)
m_e	total mass-entrainment rate of air below the level of the flame tip (kg/s)
P_s	perimeter of the vertical flue (m)
p_0	hydrostatic pressure just above floor level, see Figure 6 (N/m^2)
p_{1b}	static pressure at the base of the first box, see Figure 6 (N/m^2)
p_{na}	static pressure at the top of the n'th box (Pa)
p_{nb}	static pressure at the base of the n'th box (Pa)
p_{0n}	hydrostatic pressure outside the rack at the n'th tier (Pa)
p_n'	static pressure in the horizontal flue at the n'th tier, see Figure 13 (Pa)
p_n''	static pressure at the top of the box at the n'th tier, see Figure 13 (Pa)
q_w	heat transfer to the walls (kW/m^2)
Q	total heat release rate from the burner (kW)
Q_c	convective heat release rate from the burner (kW)
$Q_{c,exp}$	convective heat release rate based on single point measurements within the rack (kW)
$Q_{c,na}$	accumulated convective heat release rate at the top of each box at tier number n, see Figure 5 (kW)
$Q_{c,nb}$	accumulated convective heat release rate at the base of each box at tier number n, see Figure 5 (kW)
$Q_{1,2}$	volume flows in the vertical flues, see Figure 12 (m^3/s)
Re	Reynolds number
r	stoichiometric mass ratio
S	height of the boxes
$T_{n,a}$	temperature at the top of each box at tier number n, see Figure 5 (K)
$T_{n,b}$	temperature at the base of each box at tier number n, see Figure 5 (K)
T_0	ambient temperature (K)
ΔT	temperature difference (K)
u_{01}	velocity in the lowest horizontal flue (m/s)
u_{1b}	velocity at the base of the first box (m/s)
u_{na}	velocity at the top of each box (m/s)
u_{nb}	velocity at the base of each box (m/s)
u_{cold}	defined as uT_0/T (m/s)
W	width of the vertical flue
z	height from floor level (m)

ρ_o	density at ambient temperature (kg/m^3)
ρ	density within the rack storage (kg/m^3)
ϕ	air-to-fuel stoichiometric fraction

9 References

1. Ingason, H., Fire Experiments in a Two Dimensional Rack Storage, Swedish National Testing and Research Institute, SP-Report 1993:56.
2. Heskestad, G. and Yu, H-C., Fire Protection of Combustible Stacks and Mine Shafts, Phase I: Exposure-Fire Environment and Suppression, FMRC J.I. 0F0N7.RA/0E0E1.RA, 070(A), Prepared for United States Department of the Interior Bureau of Mines, FMRC, Norwood, Massachusetts, USA, October, 1982.
3. Delichatsios, M.A., Fire Protection of Fiberglass-Reinforced Plastic Stacks and Ducts, Interoffice Correspondence to File, Serial No. 22493, FMRC, Norwood, Massachusetts, USA, October, 1975.
4. Block, J.A, A Theoretical and Experimental Study of Nonpropagating Free-Burning Fires, Thirteenth Symposium (International) on Combustion, The Combustion Institute, 1971
5. Ingason, H., Rack Storage Fires, Pilot Study, SP-AR Report 1993, Technical Note, To be published, Borås, Sweden.
6. Karlsson, B., Thomas, P.H, and Holmstedt, G., Flame sizes in a small scale stack: Pilot experiments, Department of Fire Safety Engineering, Lund University, To be published in 1993, Sweden.
7. Tamanini, F., Direct Measurements of the Longitudinal Variation of Burning Rate and Product Yield in Turbulent Diffusion Flames, Combustion and Flame 51:231-243 (1983).
8. Holman, J.P., Heat Transfer, Sixth Edition, McGraw-Hill Book Company, 1986.
9. ASHRAE Handbook, 1985 Fundamentals, American Society of Heating, Refrigerating and Air-Conditioning Engineers, Inc.
10. Heskestad, G. , Peak Gas Velocities and Flame Heights of Buoyancy-Controlled Turbulent Diffusion Flames, Eighteenth Symposium (International) on Combustion, The Combustion Institute, 1981, p. 951-960.
11. Tewarson, A., Fully developed Enclosure Fires of Wood Cribs, In 20th International Symposium on Combustion, The Combustion Institute, Pittsburgh, PA, USA, 1984, p. 1555.
12. Yu, H-Z, A unified Fire Property Data Correlation Scheme for Combustibles Burning under Different Ventilation/Oxygen Concentration Conditions, Short Communication, Fire Safety Journal 20 (1993) 175-181.
13. Delichatsios, M.A., Air Entrainment into Buoyant Jet Flames and Pool Fires, The SFPE Handbook of Fire Protection Engineering, Section 1/Chapter 19, Society of Fire Protection Engineers, National Fire Protection Association.
14. B.M. Cetegen, E.E. Zukoski, and T. Kubota, Comb. Sci. and Tech., 39, 305 (1984).
15. Delichatsios, M.A. and Orloff, L., Entrainment Measurements in Turbulent Buoyant Jet Flames and Implications for Modeling, Twentieth Symp. (Int.) on Comb., Pittsburgh (1984).
16. McCaffrey, B.J. and Heskestad, G., A Robust Bi-directional Low-Velocity Probe for Flame and Fire Application, Combustion and Flame 26, 125-127, 1976.
17. Fried, E., and Idelchik, I.E., Flow Resistance, A Design Guide for Engineers, Hemisphere Publishing Corporation, USA, 1989.

SP

Swedish National Testing and Research Institute

Box 857, S-501 15 BORÅS, Sweden

Telephone: +46 33-16 50 00, Telefax: +46 33-13 55 02

SP REPORT 1993:57

ISBN 91-7848-443-X

ISSN 0284-5172